Pure appl. geophys. 158 (2001) 989–1015
0033–4553/01/060989–27 $ 1.50 + 0.20/0

Pure and Applied Geophysics

Numerical Study of the Intertropical Convergence Zone Over the Indian Ocean During the 1997 and 1998 Northeast Monsoon Episodes

ORBITA ROSWINTIARTI,[1] SETHU RAMAN,[1] and U. C. MOHANTY[2]

Abstract—The hydrostatic Naval Research Laboratory/North Carolina State University (NRL/NCSU) model was used to study the mesoscale dynamics and diurnal variability of the Intertropical Convergence Zone (ITCZ) over the Indian Ocean in the short-range period. To achieve this objective the initial conditions from two northeast monsoon episodes (29 January, 1997 and 29 January, 1998) were run for 48-hour simulations using a triple-nested grid version of the model with $1.5° \times 1.5°$, $0.5° \times 0.5°$ and $0.17° \times 0.17°$ resolutions. The 1997 case represents a typical northeast monsoon episode, while the 1998 case depicts an abnormal monsoon episode during an El Niño event.

Comparisons between the model-produced and analyzed mean circulation, wind speed, and associated rainfall for different spatial scales are presented. During the active northeast monsoon season in 1997, the major low-level westerly winds and associated high rainfall rates between 0° and 15°S were simulated reasonably well up to 24 hours. During the 1998 El Niño event, the model was capable of simulating weak anomalous easterly winds (between 0° and 15°S) with much lower rainfall rates up to 48 hours. In both simulations, the finest grid size resulted in largest rainfall rates consistent with Outgoing Longwave Radiation data.

The model performance was further evaluated using the vertical profiles of the vertical velocity, the specific humidity and temperature differences between the model outputs and the analyses. It is found that during a typical northeast monsoon year, 1997, the water vapor content in the middle troposphere was largely controlled by the low-level convergence determined by strong oceanic heat flux gradient. In contrast, during the 1998 El Niño year moisture was present only in the lower troposphere. Due to strong subsidence associated with Walker circulation over the central and eastern Indian Ocean, deep convection was not present. Finally, the diurnal variations of the maximum rainfall, vertical velocity and total heat flux were noticeable only during the 1997 northeast monsoon year.

Key words: ITCZ, Indian Ocean, Northeast monsoon, El Niño, NRL/NCSU model.

1. Introduction

The Intertropical Convergence Zone (ITCZ) is one of the most important and dynamic components of the tropical atmosphere, where the northeasterly trade winds

[1] Department of Marine, Earth and Atmospheric Sciences, North Carolina State University, Raleigh, North Carolina, USA. E-mail: sethu_raman@ncsu.edu

[2] Centre for Atmospheric Sciences, Indian Institute of Technology, NewDelhi, India.

Corresponding author: Dr. Sethu Raman, Department Marine, Earth and Atmospheric Sciences, North Carolina State University, 213 Research Building III, Centennial Campus, Raleigh, NC 27695-8208

from the Northern Hemisphere converge with the southeasterly trade winds from the Southern Hemisphere. Lying in the rising branch of both meridional Hadley and zonal Walker circulations at the equatorial trough, the ITCZ is characterized by enhanced convection, cloudiness, and rainfall and persist almost continuously around the globe throughout the year. The ITCZ plays an important role on heat budget and weather/climate not only in the tropics but in the extratropics as well. The excessive amount of heat absorbed at the surface from the tropical oceans is transported to higher altitudes through convection and latent heat release and to the extratropics through the Hadley circulation. Enhanced cloudiness associated with convective systems, moreover, contributes significantly to the planetary albedo and absorptivity of the incident solar radiation and ultimately to the regional weather and climate.

The Indian Ocean is a unique region in the world because of its largest seasonal reversing winds of the Asian-Australian (AA) monsoon phenomenon. The driving mechanisms of this monsoon circulation result from the combination of differential heating between land (orographic effect of the Tibetan Plateau and land processes such as snow cover, soil moisture, and surface albedo) and ocean, the Coriolis force and the hydrological cycle. Previous studies have encompassed a wide range of spatial and temporal scales of variability of the ITCZ and convection observed over the Indian Ocean. On the interannual time scale, anomalous warming of the sea-surface temperature (SST) in the central and eastern tropical Pacific Ocean

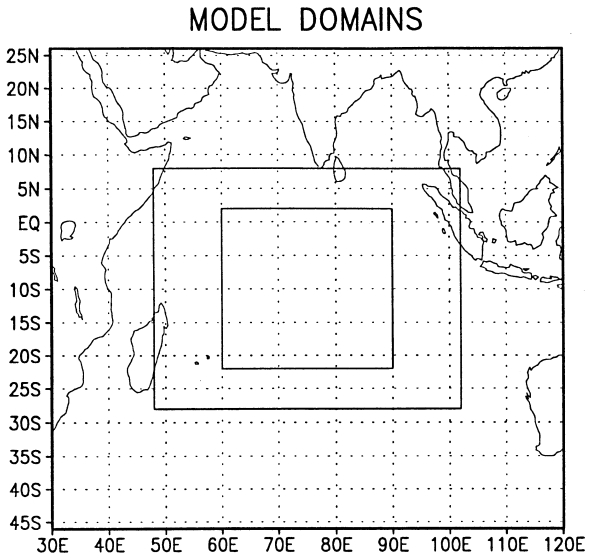

Figure 1
Model simulation domains for the Coarse-Grid Mesh (CGM), the Medium-Grid Mesh (MGM), and the Fine-Grid Mesh (FGM).

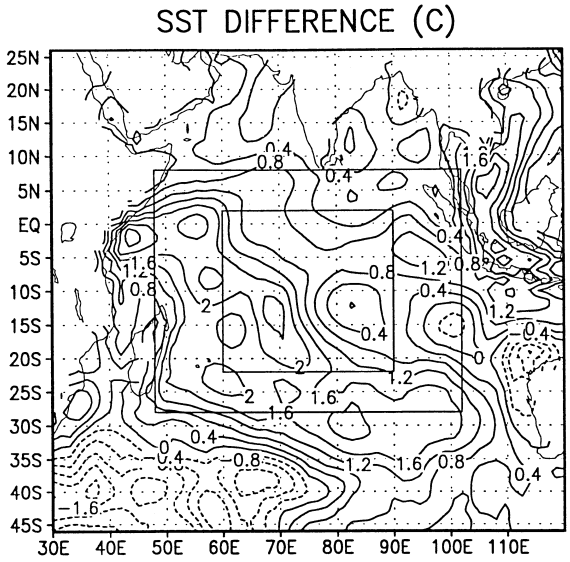

Figure 2
Distributions of SST difference (°C) between the 1998 minus 1997 simulation periods.

associated with an El Niño episode has been linked to a weakening of the AA monsoon with anomalous surface easterlies and suppressed convection over the Indian Ocean (NICHOLLS, 1989; LI, 1990; MEEHL and ARBLASTER, 1998). The sign of these changes is generally reversed during La Niño episodes. On the annual time scale, the movement of the ITCZ over the Indian Ocean is mainly caused by the difference between the land and ocean temperature (MEEHL 1987; GAUTIER *et al.*, 1998). On the interseasonal time scale, the migration of convection over the Indian Ocean is dominated by the 40–50 day Madden-Julian oscillation (MADDEN and JULIAN, 1971, 1972; LAU and CHAN, 1985; BANTZER and WALLACE, 1996). On a day-to-day basis, the mesoscale dynamic and thermal forcings over the Indian Ocean exert a significant control over the diurnal variations of vertical velocity, cloudiness and rainfall (SHARMA *et al.*, 1991; CHANG *et al.*, 1995). The nocturnal cooling over the open ocean results in enhanced convection, with maximum activity occurring generally during early morning, then decreasing throughout the day.

Although a large number of numerical simulations have been made for the southwest summer monsoon (ZWIERS, 1993; KRISHNAMURTI *et al.*, 1998), similar studies for the northeast winter monsoon are somewhat limited (DUDHIA, 1989; KITOH, 1992). The northeast monsoon plays an important role not only for regional weather and climate in the Southeast Asia and Australia regions, but also for the tropical-extratropical interactions (KRISHNAMURTI *et al.*, 1973). During a typical northeast monsoon, the main heating source is located over the equatorial belt where

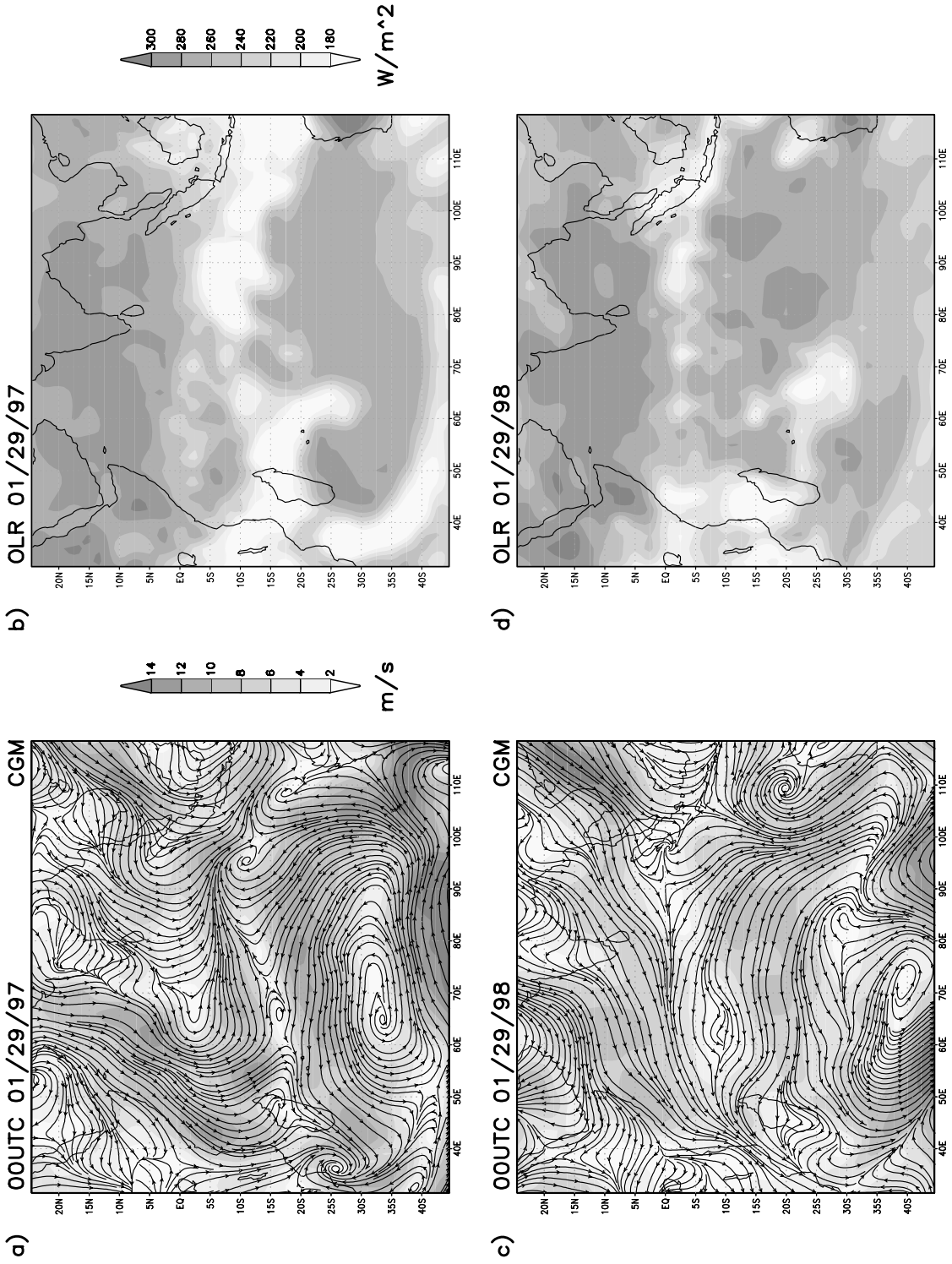
a)
00UTC 01/29/97
CGM
b)
OLR 01/29/97
c)
00UTC 01/29/98
CGM
d)
OLR 01/29/98
m/s
W/m^2

the divergent component of the motion reveals itself more prominently (LAU and CHANG, 1987). From December to January heavy rainfall and considerable latent heat release occur between the equator and 10°S when a dramatic southward shift accompained by the sudden establishment of lower-tropospheric westerlies occurs. Due to high frequency variability related to its internal dynamics, short-range monsoon forecasting has been a difficult task. Most regional forecast models over the AA monsoon region are known to have useful skill for only about 2–3 days. This rapid deterioration can be attributed to a number of factors such as uncertainly in the initial conditions, deficiencies in the internal model components, parameterization of physical processes in the forecast models and representation of orography and surface boundary conditions, such as SST variations, snow cover etc. (KRISHNAMURTI *et al.*, 1998). Although some models can predict the mean features during the period up to three days ahead, they are unable to predict monsoon onset characterized by the sudden appearance of low-level westerly winds beyond two days. For the short-range forecast, a key problem in the tropics is reduction in spinup which requires a close balance between the initial divergence, temperature and moisture fields (PURI, 1994).

As pointed out amongst others by Bony *et al.* (1997) and Lau *et al.* (1997), water vapor and clouds are not only affected by local SST changes through the activation of thermodynamics processes within the atmospheric column, they are also sensitive to many other factors that may depend only partly on the local SST. Among those factors is the large-scale atmospheric circulation, which transports heat and moisture and affects the thermodynamic stability of the atmosphere in large spatial scales. In this study, a hydrostatic model was used to simulate mesoscale circulations and associated rainfall over the Indian Ocean during a normal and an abnormal northeast monsoon episode. The model was run for 48-hours with triple-nested grids of $1.5° \times 1.5°$, $0.5° \times 0.5°$ and $0.17° \times 0.17°$ resolutions. The main objective of this study is to obtain better understanding of the maintenance and development of the interaction between the large-scale and mesoscale circulations, SST and the atmospheric convection activity, particularly for a short-range period.

This paper is organized in the following manner: Section 2 gives a brief description of the numerical model and the experiment design used in the study. Section 3 provides an overview of the synoptic initial conditions for both simulations. Comparisons between the model results and verifying analyses are presented in Section 4. Summary and conclusions of this study are given in Section 5.

◀

Figure 3
The analyzed wind circulation patterns and wind speeds at 995 hPa (initial conditions) and associated OLR distributions over the CGM domain for 00 UTC 29 January 1997 (a and b) and 00 UTC 29 January 1998 (c and d).

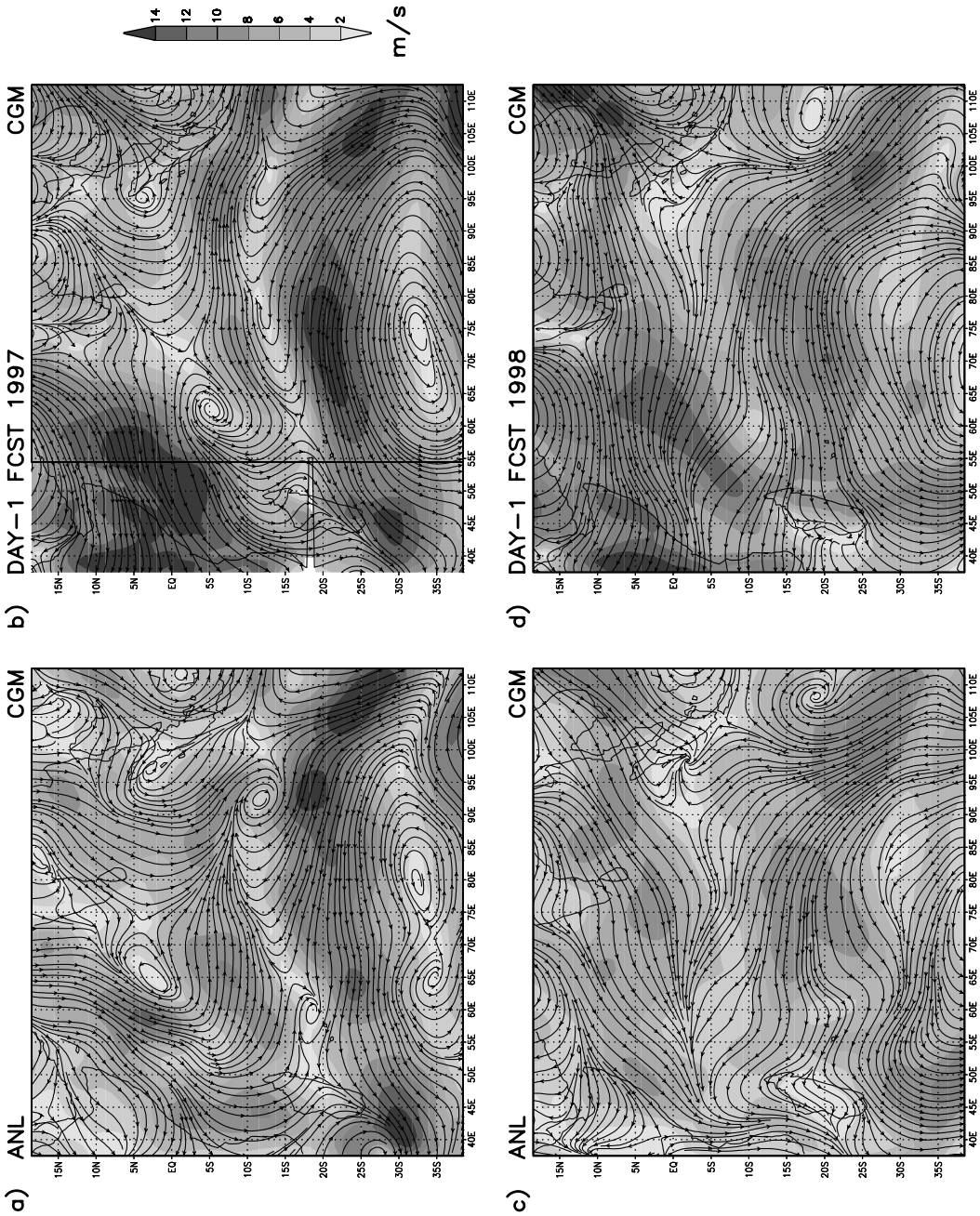
a) ANL
b) DAY−1 FCST 1997 CGM
c) ANL
d) DAY−1 FCST 1998 CGM
14 12 10 8 6 4 2
m/s

2. Description of the Model and the Experiment Design

a. Numerical Model

In this study the Naval Research Laboratory/North Carolina State University (NRL/NCSU) regional model (MADALA *et al.*, 1987) was used for the numerical simulation experiments. The primitive equations with a hydrostatic approximation are written in a non-dimensional pressure σ-coordinate system defined by $\sigma = p/p_s$, where p is the pressure and p_s is the surface pressure. By definition σ is equal to one at the surface and zero at the top of the atmosphere. This coordinate system allows the lower levels to follow the terrain and upper levels to progressively flatten as the pressure decreases toward the top of the atmosphere. There are 16 non-uniform σ levels between the surface and 50 hpa. Seven levels are located in the lowest 850 hpa and nine levels above it.

The prognostic equations included in the primitive equations are the zonal and meridional momentum equations, thermodynamic equation, moisture continuity equation and surface pressure tendency equation. The diagnostic equations exist for the vertical motion (continuity equation) and geopotential height (hydrostatic equation).

The time differencing scheme used in this model is a split-explicit method. This method utilizes different time steps for slow-moving Rossby modes and fast-moving gravity modes in the prognostic equations. Fast-moving modes use smaller time steps than do slow-moving modes. Appropriate time steps satisfying Courant-Fredrichs-Levy (CFL) criteria are used for the fast-moving modes.

A type-C Arakawa staggering is applied for the horizontal velocity variables with respect to the non-velocity variables. The surface pressure, specific humidity, temperature, geopotential height and vertical velocity ate specified at the same horizontal points, while zonal and meridional winds are interlaced between them. The spatial differencing scheme used for the conservation of energy, mass, and momentum equations is of second-order accuracy.

The latest version of this model contains a multiple nesting capability of up to three domains run simultaneously with a one-way nesting mode. One-way nesting involves prescribing boundary values for a sub-domain from its mother domain interior, while no feedback occurs to the mother domain. The horizontal grid size and time step used for each sub-domain are one-third of its mother domain. For this study the grid size for the Coarse Grid Mesh (CGM), the Medium Grid Mesh (MGM) and the Fine Grid Mesh (FGM) were $1.5° \times 1.5°$ ($\sim$166 km $\times$ 166 km),

◀

Figure 4

The analyzed and simulated streamlines and wind speeds at 995 hPa over the CGM domain with $1.5° \times 1.5°$ resolution for 00 UTC 30 January 1997 (a and b) and 00 UTC 30 January 1998 (c and d).

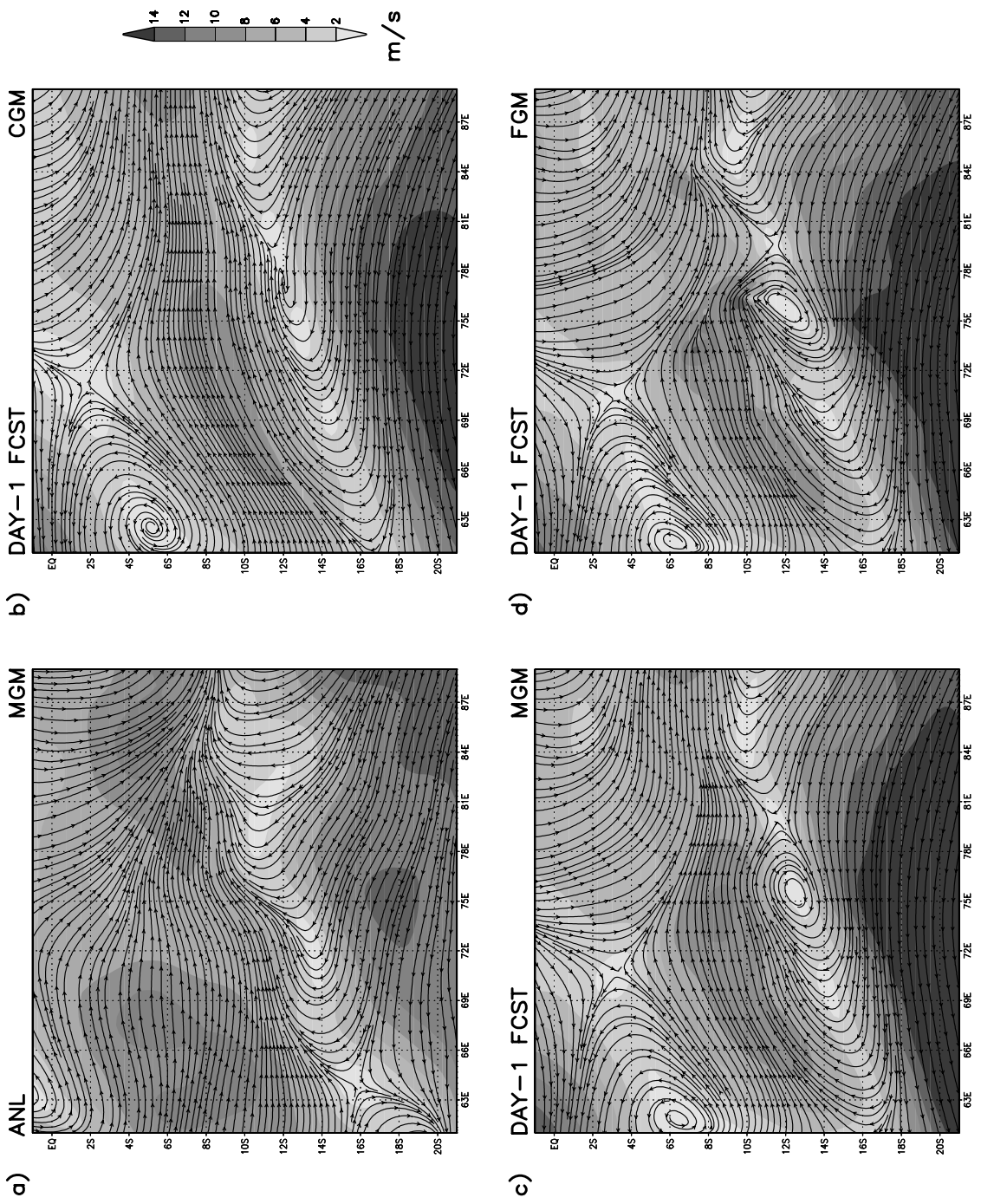
a) ANL
MGM
b) DAY−1 FCST
CGM
c) DAY−1 FCST
MGM
d) DAY−1 FCST
FGM
14 12 10 8 6 4 2
m/s
EQ 2S 4S 6S 8S 10S 12S 14S 16S 18S 20S
63E 66E 69E 72E 75E 78E 81E 84E 87E

0.5° × 0.5° (~55 km × 55 km) and 0.17° × 0.17° (~19 km × 19 km) with time steps of 300 sec., 100 sec. and 33 sec., respectively.

The lateral boundary conditions for the three domains are calculated by the Davies scheme (DAVIES, 1976, 1983). In this scheme, any independent variable a can be written as

$$a = (1 - \alpha)a_m + \alpha a_b$$

where the subscript m represents mode-computed values and subscript b represents the boundary layer values obtained either from observations or a coarser version of the model. The merging is done over six grid points at the boundaries of three domains. The α is defined as a quadratic function of the minimum distance from the lateral boundary in units of the grid spacing. At each time step, the boundary values a_b for the coarse grid are obtained through a linear interpolation in time from the input data at 24-hour intervals. For the FGM domain, lateral boundary conditions a_b are obtained through a linear interpolation in time and space from the CGM domain. At the model top and bottom, boundary conditions for vertical velocity $\dot{\sigma}$ is zero.

In the model, the surface layer is parameterized by a similarity theory (MONIN and YAGLON, 1971), while the mixed layer is parameterized by the turbulence kinetic energy and its dissipation rates ($E - \varepsilon$) closure scheme (HOLT and RAMAN, 1998). Moreover, the ground temperature is modeled using two-layer soil slabs (BLACKADAR, 1976).

For this study, the convective precipitation is parameterized by the Kuo-Anthes cumulus parameterization scheme (KUO, 1974; ANTHES, 1977), while the non-convective precipitation is based on MANABE *et al.* (1965). In addition to the cumulus parameterization scheme, the model physics includes grid-scale precipitation, dry convection, diffusion processes, latent heat, sensible heat, and momentum exchange between the boundary layer and the underlying surface using the similarity theory of BUSINGER *et al.* (1971). The soil-vegetation parameterization scheme of NOILHAN and PLANTON (1989) is used. The short- and longwave radiative processes in the atmosphere are not included in this model.

b. Experiment Design

The model domains for the CGM, MGM and FGM are shown in Figure 1. The CGM domain covers from 30°E to 120°E between 26°N and 46°S, the MGM domain from 48°E to 102°E between 8°N and 28°S and the FGM domain from 60°E to 90°E between 2°N and 22°S. The latter is located over the Indian Ocean.

Two northeast monsoon events selected for this study are that of 00 UTC 29–00 UTC 31 January, 1997 and 00 UTC 29–00 UTC 31 January, 1998. These periods

◀

Figure 5
The analyzed (a) and simulated streamlines and wind speeds at 995 hPa for 00 UTC 30 January 1997 over the FGM domain for 1.5° × 1.5°(b), 0.5° × 0.5° (c), and 0.17° × 0.17° (d) resolutions.

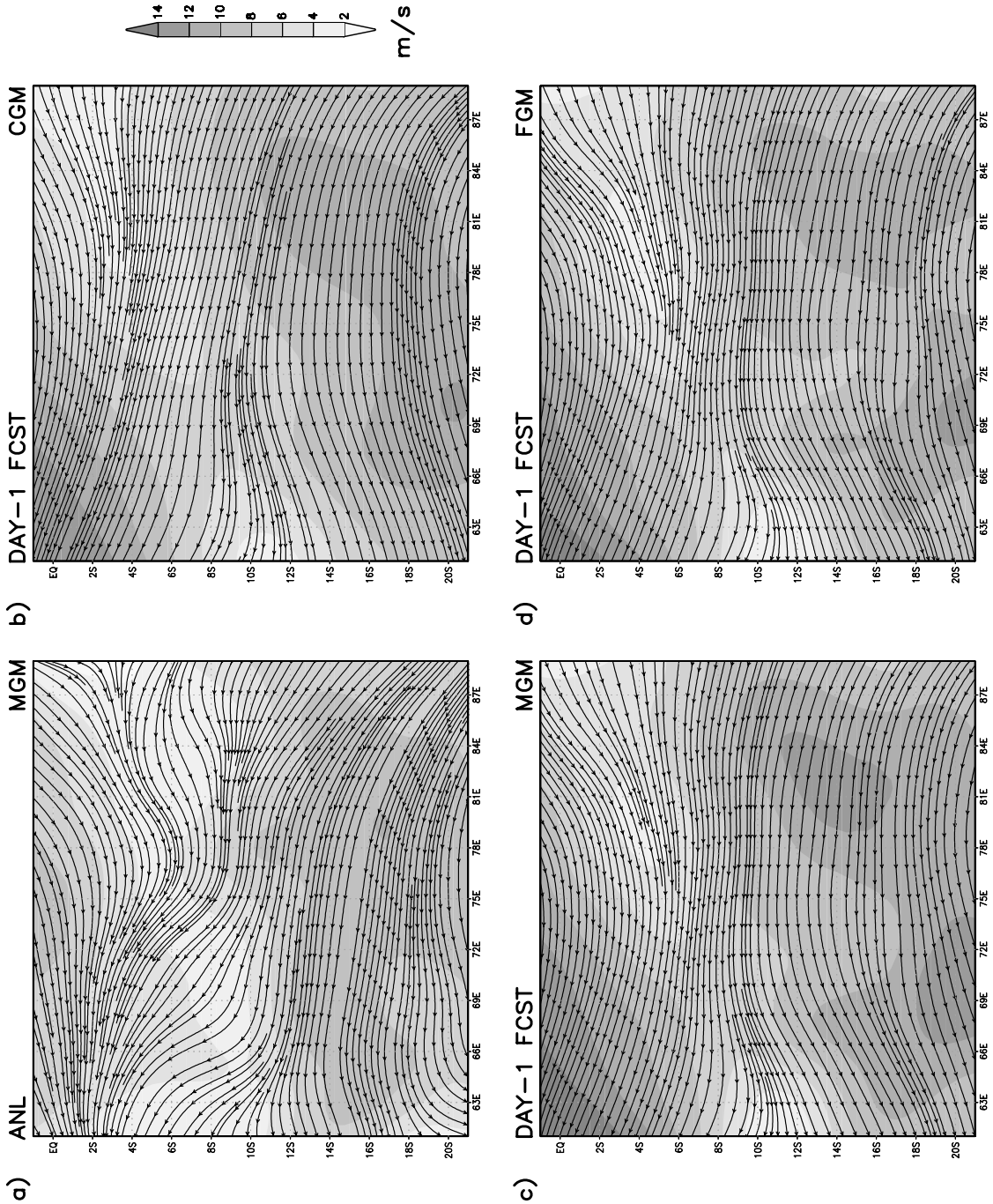
a) ANL
MGM
b) DAY−1 FCST
CGM
c) DAY−1 FCST
MGM
d) DAY−1 FCST
FGM
14 12 10 8 6 4 2
m/s
EQ 2S 4S 6S 8S 10S 12S 14S 16S 18S 20S
63E 66E 69E 72E 75E 78E 81E 84E 87E

were chosen because they exhibited the main features of a typical northeast monsoon episode during a normal year and during an abnormal episode in an El Niño year.

Inputs for this model can be categorized into three types: 1) Meteorological data consisting of zonal and meridional components of wind, temperature, humidity, surface pressure, eigenvalues for each level, SST, and boundary conditions for the coarse domain; 2) surface data of topography, albedo, roughness length, soil type, surface ground water and subsurface ground water; and 3) vegetation data of land use type, vegetation cover, leaf area index, and minimum stomatal resistance of vegetation. We utilized meteorological data sets from the European Centre for Medium-Range Weather Forecasts (ECMWF) analyses of $2.5° \times 2.5°$ grid at 15 pressure levels on 00 UTC 29 January, 1997 and on 00 UTC 29 January, 1998 to specify the initial conditions. The surface topography distribution was obtained from the Navy 5′ global topography data set. The SSTs were taken from the weekly averaged optimum interpolation data sets. These data were available at $1° \times 1°$ resolution. During the model integration, the SSTs were kept constant. Surface and vegetation properties were obtained from various data archives at the National Center for Atmospheric Research (NCAR) with resolutions ranging from $0.17° \times 0.17°$ to $1° \times 1°$. These data were then interpolated into the model's grid sizes using a bicubic polynomial technique.

Since direct measurements of rainfall are scarce in the tropical ocean regions, we used daily Outgoing Longwave Radiation (OLR) data as the indicator of deep convection and thereby rainfall. In the tropics, OLR is governed primarily by cloud-top temperatures. Therefore, low OLR values related to high cloud tops are correlated with deep convection and thus with the ITCZ while high OLR values with clear conditions (MEEHL, 1987; VINCENT, 1994). The OLR data were obtained from the NOAA-CIRES Climate Diagnostic Center at a resolution of $2.5° \times 2.5°$.

3. Overview of Synoptic Initial Conditions

The main difference between the 1997 and 1998 northeast monsoon conditions over the Indian Ocean was due to the differences in the distribution and location of maximum SST values. Figure 2 shows the spatial distribution of the SST difference between the 1998 minus 1997 simulation periods. During the 1998 El Niño event warmer SSTs with a maximum magnitude of about 2.4°C occurred over the western Indian Ocean region.

The analysed streamlines and wind speeds at 995 hPa for 00 UTC 29 January, 1997 and for 00 UTC 29 January, 1998 used as the initial conditions and the

◀

Figure 6
As in Fig. 5, except for 00 UTC 30 January 1998.

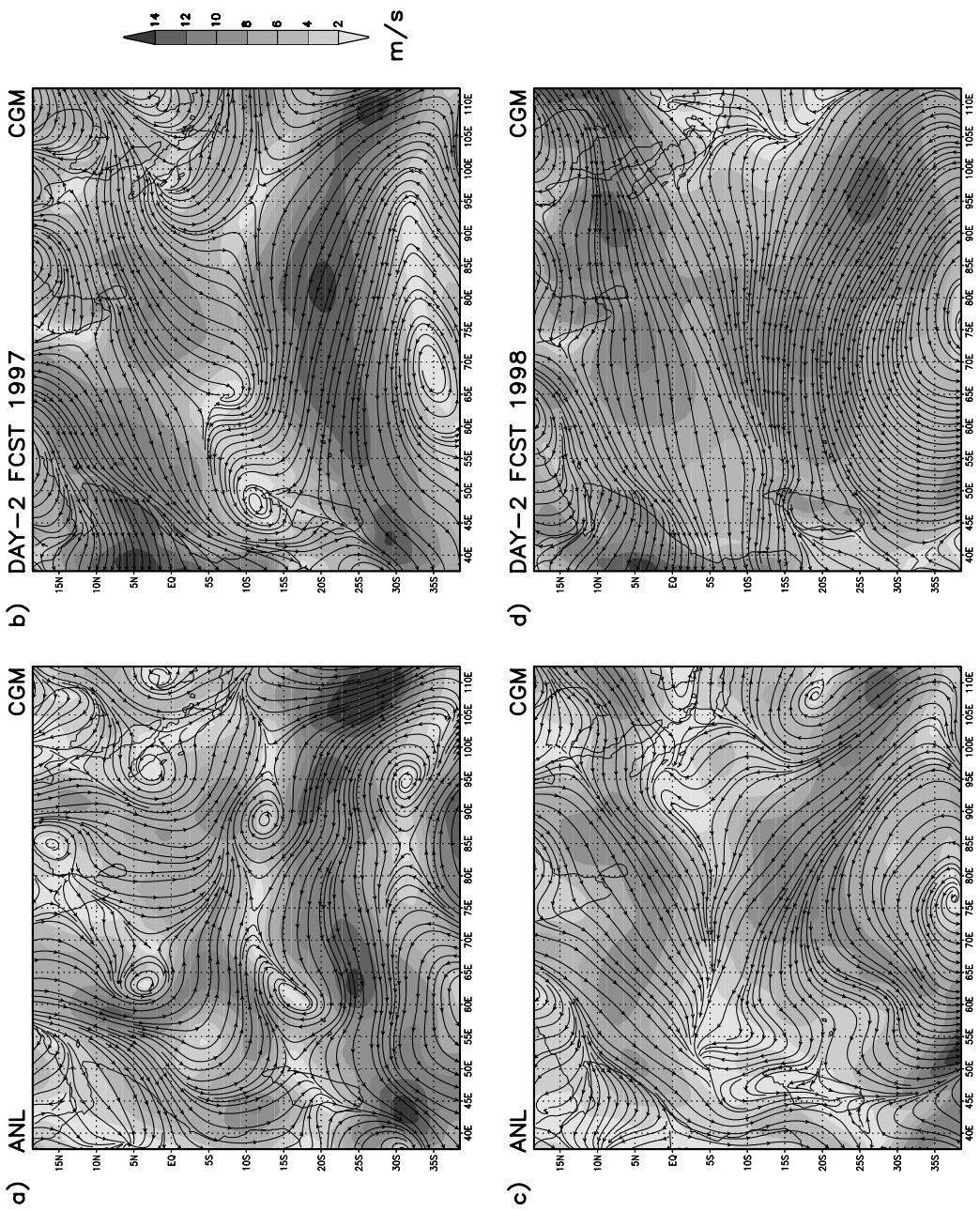
14
12
10
8
6
4
2
m/s
a) ANL
CGM
b) DAY−2 FCST 1997
CGM
c) ANL
CGM
d) DAY−2 FCST 1998
CGM

corresponding OLR distributions over the CGM domain are shown in Figures 3a–d. The low-level flow fields at 00 UTC 29 January, 1997 (Fig. 3a) were dominated by the southeasterly trade winds over the southern Indian Ocean and the northerly/northeasterly trade winds over the southern Asia land mass. These winds converged near 5°S resulting in westerly winds (with amplitudes of 6 to 12 ms^{-1}). It should be noted that the strongest winds did not occur where the winds were convergent. During this day, the ITCZ was best developed over the southern Indian Ocean from the equator to 15°S as confirmed by the OLR distribution with OLR $\leq$ 240 Wm^{-2} (Fig. 3b). Within the next two days, winds and the convective activity intensified, indicating an active northeast monsoon period.

In contrast, the surface convergence winds (with amplitudes from 6 to 10 ms^{-1}) over the equatorial Indian Ocean on 29 January, 1998 were mainly westward (Fig. 3c). From Figure 3d, it is apparent that the ITCZ over this region during this time was least organized. These low-level easterlies and weak convection persisted until 00 UTC 31 January, 1998. During an El Niño event an eastward displacement of the ascending branch of the Walker circulation over the eastern Indian Ocean induces subsidence and consequent dry conditions. The rising motion and convection, on the other hand, are located over eastern Africa and western Indian Ocean. Therefore, anomalous easterlies are generally observed over the equatorial Indian Ocean during an El Niño event, particularly in boreal winter (WRIGHT *et al.*, 1988; WEBSTER *et al.*, 1999; SAJI *et al.*, 1999). Weakening of the easterly winds over the Indian Ocean commonly follows the weakening of the easterly winds over the eastern Pacific Ocean (LAU, 1982).

4. Discussion of Results

In order to understand the dynamic and thermodynamic processes associated with the ITCZ in two contrasting oceanic environments, simulations of wind fields, precipitation and surface fluxes are examined. Results of numerical simulations from the 1997 normal and the 1998 abnormal El Niño years are presented and compared.

a. Streamlines and Wind Speeds

Figures 4a–d illustrate the large-scale analyzed and simulated streamlines and wind speeds at 995 hPa for day 1 of simulations (00 UTC 30 January, 1997 and 00 UTC 30 January, 1998) over the CGM domain. A reasonable correspondence

◀

Figure 7

The analyzed and simulated streamlines and wind speeds at 995 hPa over the CGM domain with 1.5° × 1.5° resolution for 00 UTC 31 January 1997 (a and b) and 00 UTC 31 January 1998 (c and d).

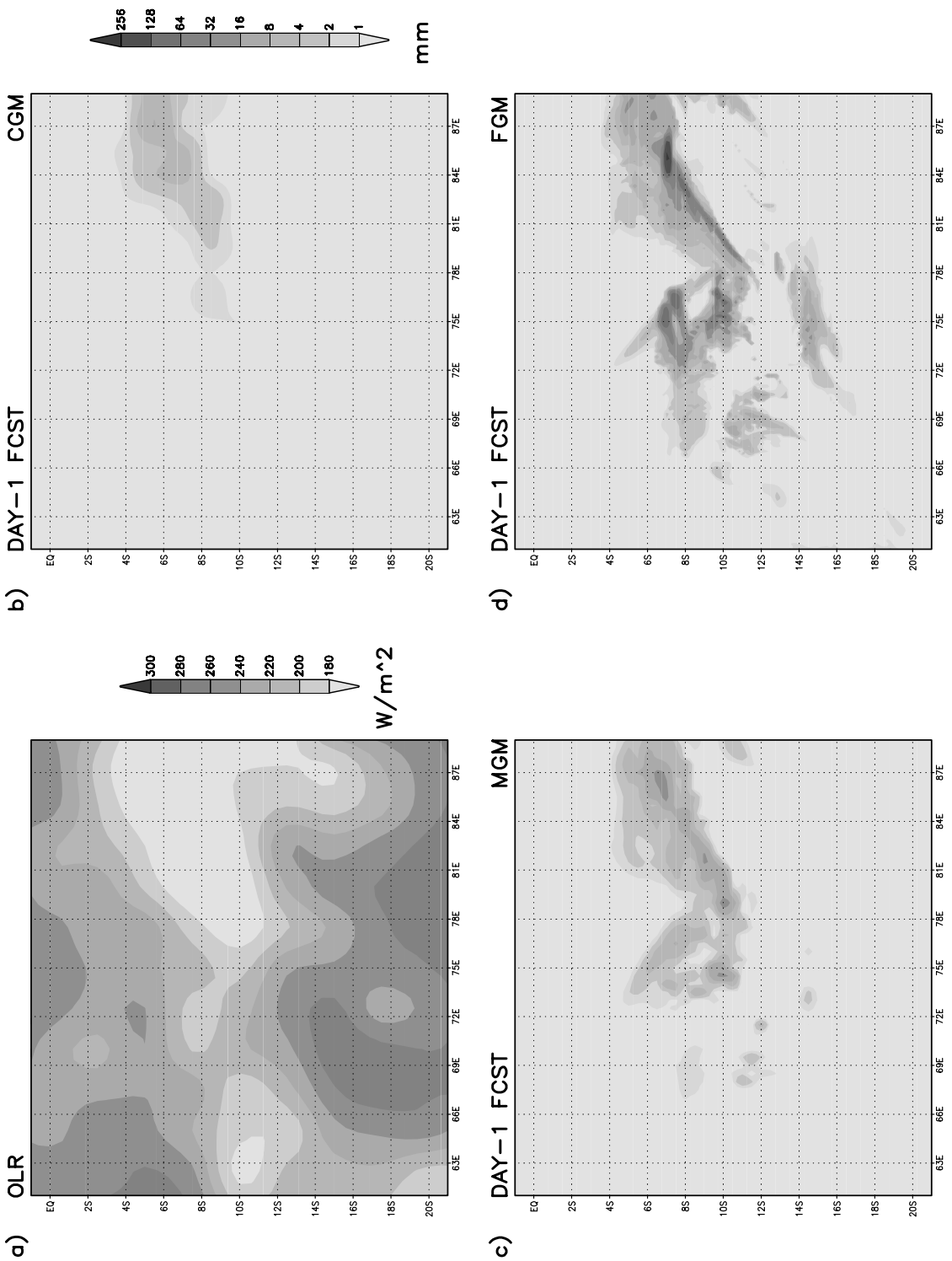
a)
OLR
300
280
260
240
220
200
180
W/m^2
b)
DAY−1 FCST
CGM
256
128
64
32
16
8
4
2
1
mm
c)
DAY−1 FCST
MGM
d)
DAY−1 FCST
FGM
EQ
2S
4S
6S
8S
10S
12S
14S
16S
18S
20S
63E
66E
69E
72E
75E
78E
81E
84E
87E

between the simulated and analyzed flow features exists, which includes the low-level convergent westerly winds between 5°S and 15°S at 00 UTC 30 January, 1997, the surface convergent easterly winds from the equator to 5°S at 00 UTC 30 January, 1998, and the high-pressure system over the subtropical Indian Ocean for both cases. The model was also able to simulate the wind speeds of roughly 6 to 12 ms^{-1} for 00 UTC 30 January, 1997 and 6 to 10 ms^{-1} for 00 UTC 30 January, 1998. However, northeasterly winds over the Arabian Sea were not simulated properly in both cases.

In order to evaluate the effect of different model resolutions, simulations from $1.5° \times 1.5°$, $0.5° \times 0.5°$, and $0.17° \times 0.17°$ nested grids are presented only over the FGM domain, i.e., over the Indian Ocean. Figures 5a–d show the analyzed and simulated streamlines and wind speeds at 995 hPa for 00 UTC 30 January, 1997 over the FGM domain with different horizontal grid resolutions. Although there were minor differences, it is clear from these figures that the locations of the surface westerly convergence (with amplitudes of 6 to 12 ms^{-1}) over the southern equatorial Indian Ocean, in the domain (17°S, 61°E) to (12°S, 89°E), were simulated reasonably well in all resolutions. As the resolution increased, the model was able to predict cyclonic eddies near 12°S. Nevertheless, since the location of a cyclonic circulation at 2.5°N was not accurately predicted, the forecast for the westerly winds between 62.5°E and 72°E near 6°S was quite different from the analysis.

The overall circulations and wind speeds at 00 UTC 30 January, 1998 were also in good agreement with the analysis (Figs. 6a–d). The main feature to note is that the easterly low-level flows (with amplitudes of 6 to 10 ms^{-1}) were dominant in this region at this time. These easterly flows provide an indication that the ascending branch of the Walker circulation was located over eastern Africa and the western Indian Ocean.

Figures 7a–d exhibit the analyzed and simulated streamlines and wind speeds at 995 hPa for day 2 integration of the model (00 UTC 31 Jaunuary, 1997 and 00 UTC 31 January, 1998) over the CGM domain. It is found that at 00 UTC 31 January, 1997 the convergent westerly winds (with amplitudes of 8 to 10 ms^{-1}) were not properly simulated. Instead, the model tended to produce easterly winds (with amplitudes of 4 to 8 ms^{-1}). These indicate the inability of a coarse resolution regional model to generate and maintain the low-level westerly winds reaching 48 hours of integration. Additionally, eddies of low-pressure systems were missing from this simulation. As mentioned earlier, a major problem in monsoon forecasting is the spin up of the model. Spin up time is generally larger for the tropics as compared to mid-latitudes. Moreover, as the winds strengthened, the model is not able to maintain the

◀

Figure 8
The OLR distribution (a) and simulated accumulated rainfall for a period of 24 hours ending at 00 UTC 30 January 1997 over the FGM domain for $1.5° \times 1.5°$ (b), $0.5° \times 0.5°$ (c), and $0.17° \times 0.17°$ (d) resolutions.

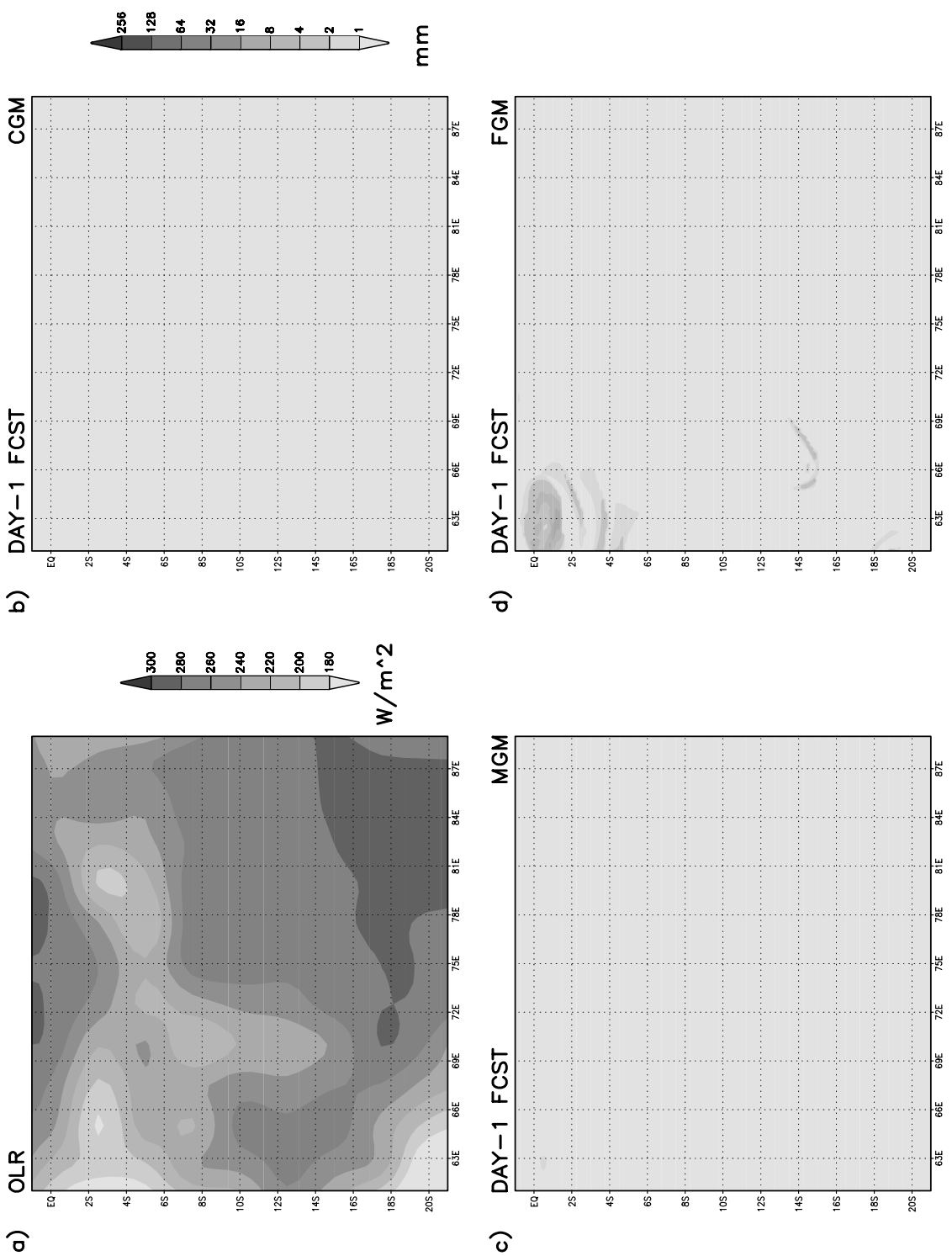
a)
OLR
300
280
260
240
220
200
180
W/m^2
b)
DAY−1 FCST
CGM
256
128
64
32
16
8
4
2
1
mm
c)
DAY−1 FCST
MGM
d)
DAY−1 FCST
FGM
EQ
2S
4S
6S
8S
10S
12S
14S
16S
18S
20S
63E
66E
69E
72E
75E
78E
81E
84E
87E

balance between dynamic and thermodynamic processes. On the other hand, the streamlines and wind speeds (with amplitudes between 6 and 8 ms^{-1}) for 00 UTC 31 January, 1998, in general, were simulated reasonably well. Since the winds did not strengthen or weaken, the model could handle low-level easterlies reasonably. Notable differences between the simulation and the analysis are again the northerly/northeasterly winds over the Arabian Sea.

b. Rainfall

Past studies have shown that the forecast of monsoon rainfall in the tropics is very sensitive to the cumulus parameterization and its coupling with other model physics used in the model (SLINGO *et al.*, 1998 and ZANG, 1994). The Kuo-Anthes scheme used in this model accounts for the effect of changes in the large-scale humidity and temperature fields on the cumulus convection (ANTHES, 1997).

The simulated accumulated rainfall valid for 00 UTC 30 January, 1997 along with the OLR distribution over the FGM domain are shown in Figures 8a–d. Overall, the model captured the maximum rainfall over the eastern regions of the FGM domain centered around (8°S, 84°E). This is consistent with the low values of observed OLR. Considerable increase in maximum rainfall, 8 mm for CGM to 200 mm for FGM, was predicted as the model resolution increased. Moreover, rainfall distributions exhibited a clear rain band structure along the ITCZ which appears to be more realistic.

Figures 9a–d illustrate the OLR distribution and simulated accumulated rainfall at 00 UTC 30 January, 1998. It is clear from these results that overall magnitude were considerably less than those for 00 UTC 30 January, 1997. The rain location was mainly in the western part of the FGM domain close to the east coast of Africa. The heaviest rainfall for the CGM was only 0.5 mm, while it was 10 mm for the FGM. Though the SSTs over this region were relatively higher, the decrease in rainfall is mainly attributed to the absence of the ITCZ and increased subsidence over the central-eastern Indian Ocean generated by the strong rising motion over western Africa. Such circulation is typical during El Niño years due to a shift in Walker circulation as discussed earlier.

The OLR distribution and simulated accumulated rainfall for 00 UTC 31 January, 1997 and 00 UTC 31 January, 1998 are given in Figures 10a–d and Figures 11a–d, respectively. For day 2 stimulation at 00 UTC 31 January, 1997, rainfall reaching 200 mm occurred in the eastern Indian Ocean and was in good agreement with low OLR values. Although the low-level winds were not simulated well at this time, there was definitely an improvement in the rainfall prediction. At 00 UTC 31

◀

Figure 9
As in Fig. 8, except for 00 UTC 30 January 1998.

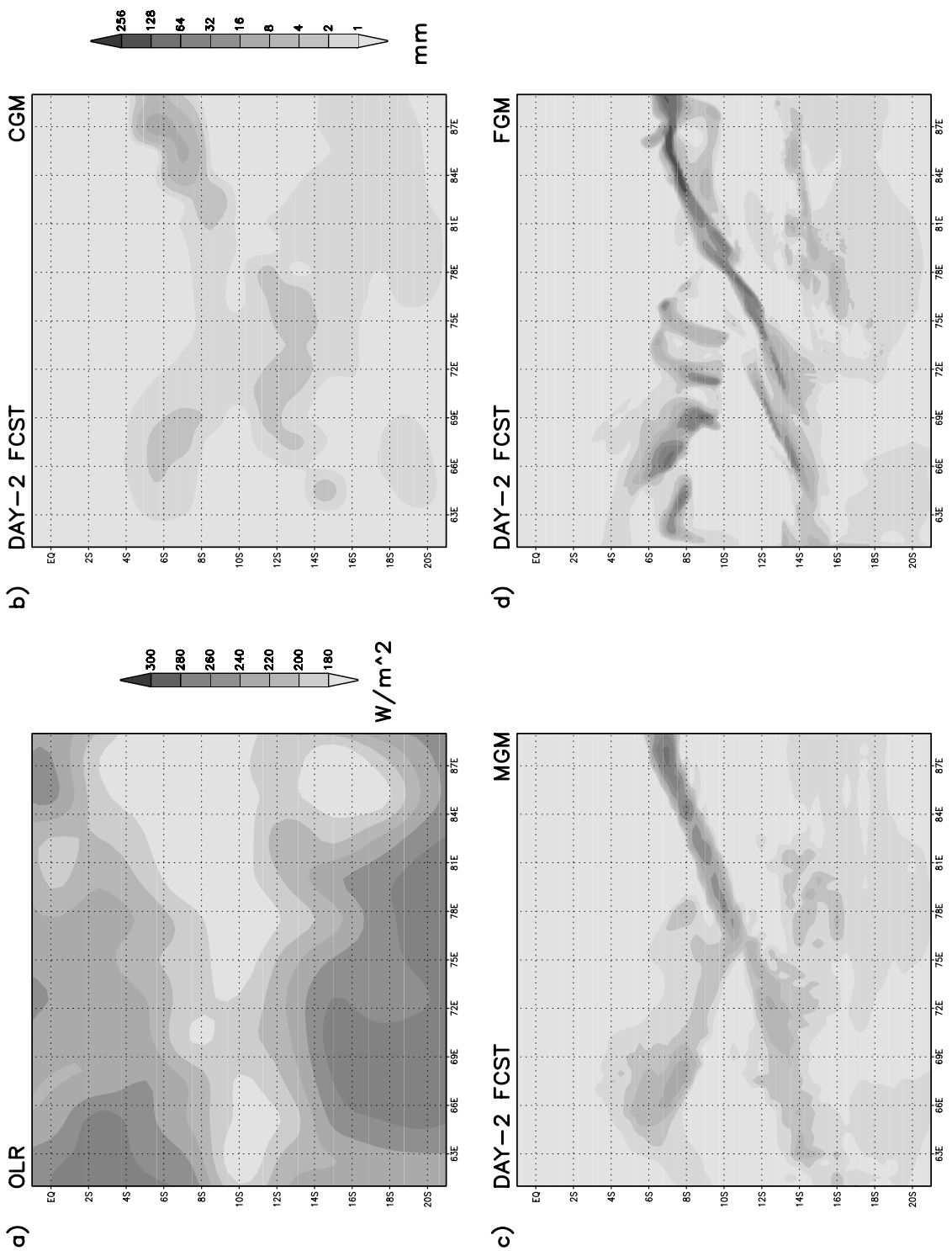
a)
OLR
300
280
260
240
220
200
180
W/m^2
b)
DAY−2 FCST
CGM
256
128
64
32
16
8
4
2
1
mm
c)
DAY−2 FCST
MGM
d)
DAY−2 FCST
FGM
EQ
2S
4S
6S
8S
10S
12S
14S
16S
18S
20S
63E
66E
69E
72E
75E
78E
81E
84E
87E

January, 1998 the area of rain had moved slightly to the south compared to the day before. Considerably more rainfall in the order of 50 mm was simulated during this time, consistent with the observed OLR values.

c. Spatial Distribution of Mean Kinetic Energy and Total Heat Flux

To understand the effect of mesoscale circulations and the SST on the rainfall distribution over the ITCZ region, the spatial distribution of simulated mean kinetic energy and total surface heat flux (latent plus sensible heat flux) for day 1 simulation are presented.

Figures 12a–b display daily mean (obtained by averaging values simulated every hour) kinetic energy predicted over the FGM domain for 00 UTC 30 January, 1997 and 00 UTC 30 January, 1998, respectively. Strong gradients of kinetic energy (with amplitudes of 10 to 90 $m^2\ s^{-2}$) simulated over the ITCZ regime at 00 UTC 30 January, 1997 (Fig. 12a) corresponded to strong wind speed gradient along a band of the ITCZ. As the spatial resolution in the model domain was increased, this kinetic energy gradient became stronger (not shown). The generation of kinetic energy gradient in this region is a manifestation of sharp contrasts in pressure difference between subtropical high-pressure and equatorial low-pressure systems. During the 1998 El Niño event, gradient of the kinetic energy was not simulated in any domain excepting a small area in the western FGM domain (Fig. 12b). An overall reduction of kinetic energy over the entire domain is also apparent. These results suggest that a uniform high-pressure system over the central-eastern Indian Ocean produced more moderate wind speeds.

Figures 13a–b show daily mean simulated total surface heat flux for 00 UTC 30 January, 1997 and 30 January, 1998, respectively. There is a general similarity between the heat flux (in the range of 100 to 250 Wm^{-2}) and the kinetic energy patterns for 00 UTC 30 January, 1997. The strong surface heat flux gradient indicated substantial transport of heat and moisture form ocean to atmosphere. This strong heat flux gradient, combined with strong kinetic energy on either side of the ITCZ, obviously played an important role in stimulating strong convection and rainfall along the ITCZ region. In contrast, the magnitudes of total heat flux for 00 UTC 30 January, 1998 (Fig. 13b) in general were relatively higher (maximum value = 280 Wm^{-2}) than those for 00 UTC 30 January, 1997, although with a weaker horizontal gradient. It is obvious that the direct response of local heating induced by increased SST during the El Niño event resulted in higher heat flux. However, lack of strong convergence (Fig. 12b) resulted in reduced rainfall simulation particularly over the eastern Indian Ocean.

◀

Figure 10
As in Fig. 8, except for 00 UTC 31 January 1997.

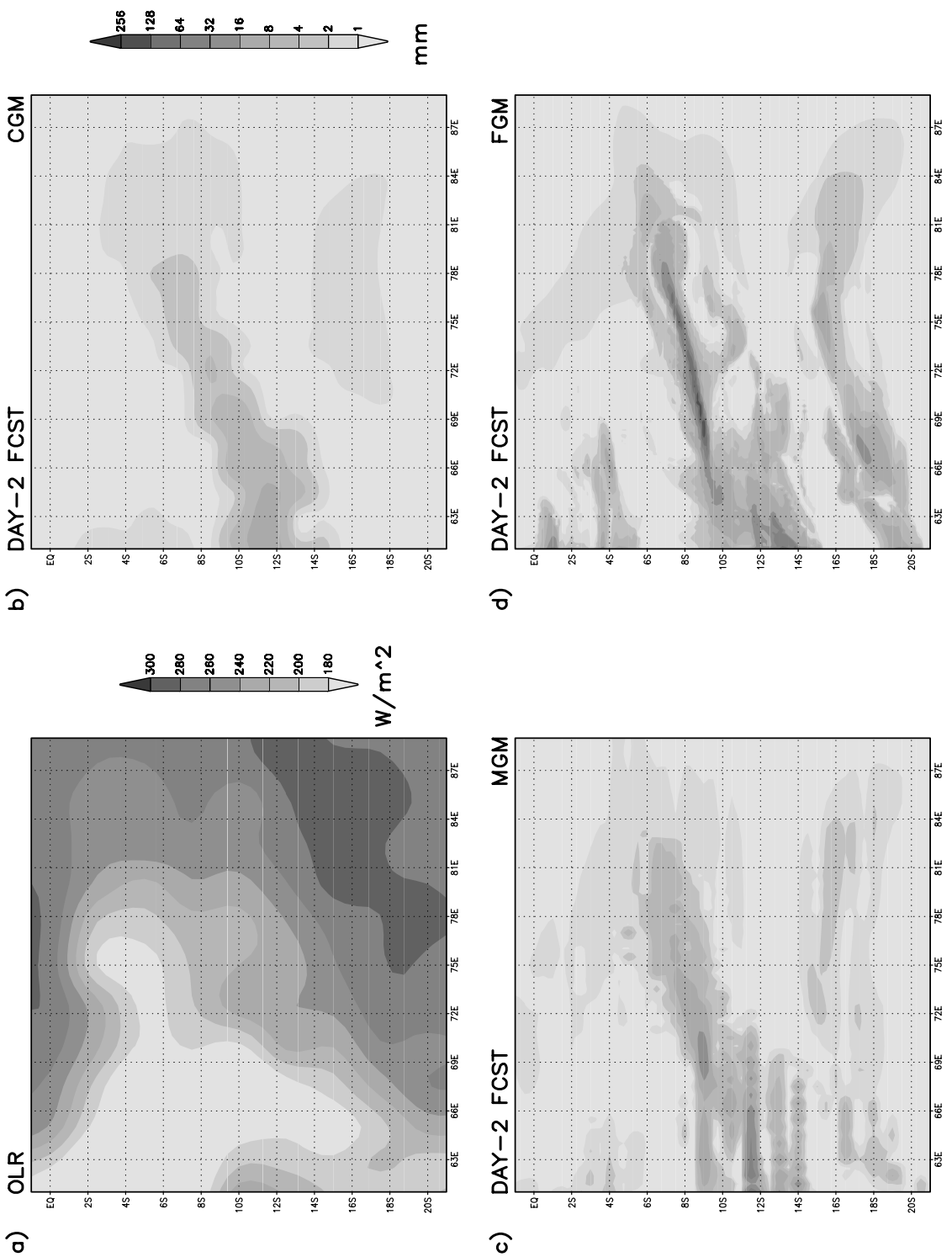
a)
OLR
300
280
260
240
220
200
180
W/m^2
b)
DAY−2 FCST
CGM
256
128
64
32
16
8
4
2
1
mm
c)
DAY−2 FCST
MGM
d)
DAY−2 FCST
FGM
EQ
2S
4S
6S
8S
10S
12S
14S
16S
18S
20S
63E
66E
69E
72E
75E
78E
81E
84E
87E

d. Diurnal Variation of Rainfall, Vertical Velocity and Total Heat Flux

The previous sections discussed how the dynamic and thermodynamic spatial variations impact the tropospheric moisture and temperature changes in the ITCZ region. In this section hourly values of maximum rainfall, minimum vertical velocity ω and maximum total heat flux as a function of Local Solar Time (LST) are examined to study the diurnal cycle. Figures 14a–c and 15a–c summarize these cycles for 29–31 January, 1997 and 29–31 January, 1998, respectively.

In general, distinct diurnal variations were found during a typical northeast monsoon (Figs. 14a–c) as compared to El Niño year (Figs. 157a–c). During a typical northeast monsoon with distinct ITCZ features, enhanced rainfall activity (minimum ω) is predicted during early morning hours, with a maximum rate of 55 mm hr^{-1} around 05 LST and a suppressed rainfall rate (maximum ω) at nearly 17 LST (Figs. 14a–b). This result is in agreement with previous studies (e.g., EMANUEL and RAYMOND, 1994). Although simulated maximum total surface heat flux experienced similar variations (Fig. 14c), its fluctuations are not correlated with variations in rainfall. One possible reason is that the difference between sea and air temperatures is directly proportional to the sensible heat flux across the air-sea interface, however variations of latent heat flux depend on variations of wind speeds. The simulated heat flux maximized around 20 LST when the sea-air temperature difference reached the maximum and lowest around 09 LST. During the El Niño event no significant diurnal cycles were found over the central Indian Ocean where strong large-scale subsidence was present. Rainfall started after 34 hours of simulation corresponding to minimum ω (Figs. 15a–b). In general, larger surface heat flux with a maximum value on the order of 525 Wm^{-2} was observed over the Indian Ocean during the 1998 El Niño event.

5. Summary and Conclusions

This paper presents simulations of major circulations and associated rainfall of the northeast monsoon during January, 1997 and January, 1998 using a hydrostatic model. In this study the objective is to simulate the dynamic and thermodynamic processes associated with enhanced and suppressed convection.

In general, the model was able to predict major westerly winds and associated rainfall over the central-eastern Indian Ocean during an active 1997 northeast monsoon with well established ITCZ extending to 24-hour simulation. Overall, rainfall was also simulated reasonably well consistent with OLR data. The distribution of rainfall indicated strong relationships between low-level convergence,

◀

Figure 11
As in Fig. 8, except for 00 UTC 31 January 1998.

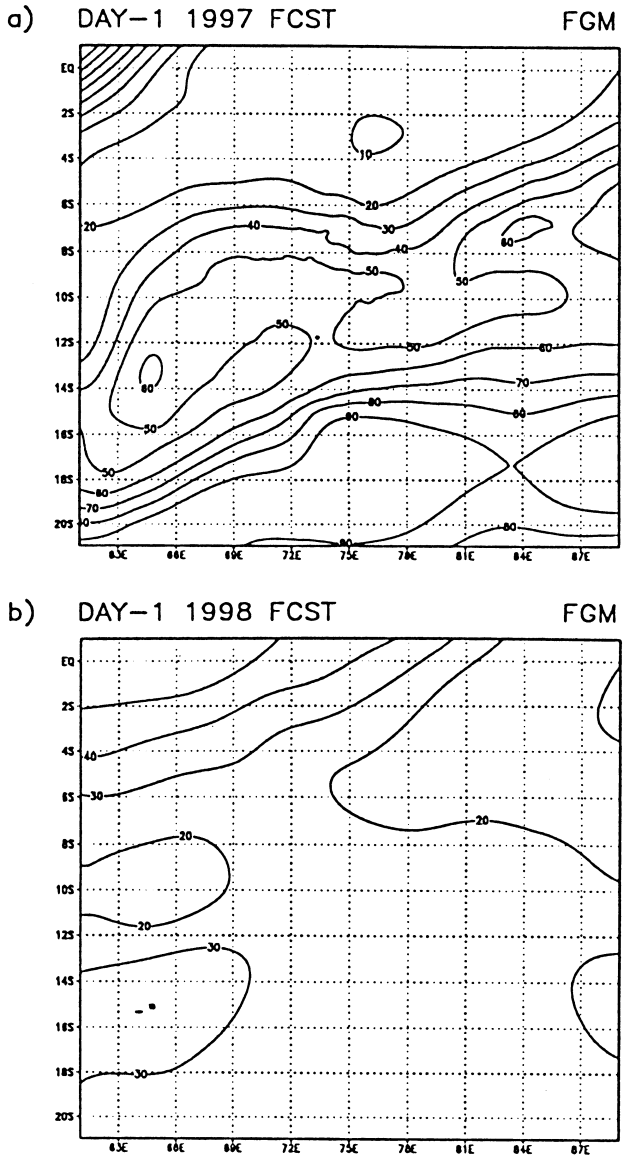

Figure 12
Distributions of simulated mean kinetic energy (m^2s^2) at 995 hPa over the FGM domain with 0.17° × 0.17° resolution for 00 UTC 30 January, 1997 (a) and 00 UTC 30 January, 1998 (b).

rising motion and moisture content. While gradient of surface heat flux provided moisture near the surface, the low-level convergence is an important mechanism for the moisture supply in the upper troposphere. For the 48-hour simulation, the model failed to simulate strengthened westerly winds. A number of factors could be

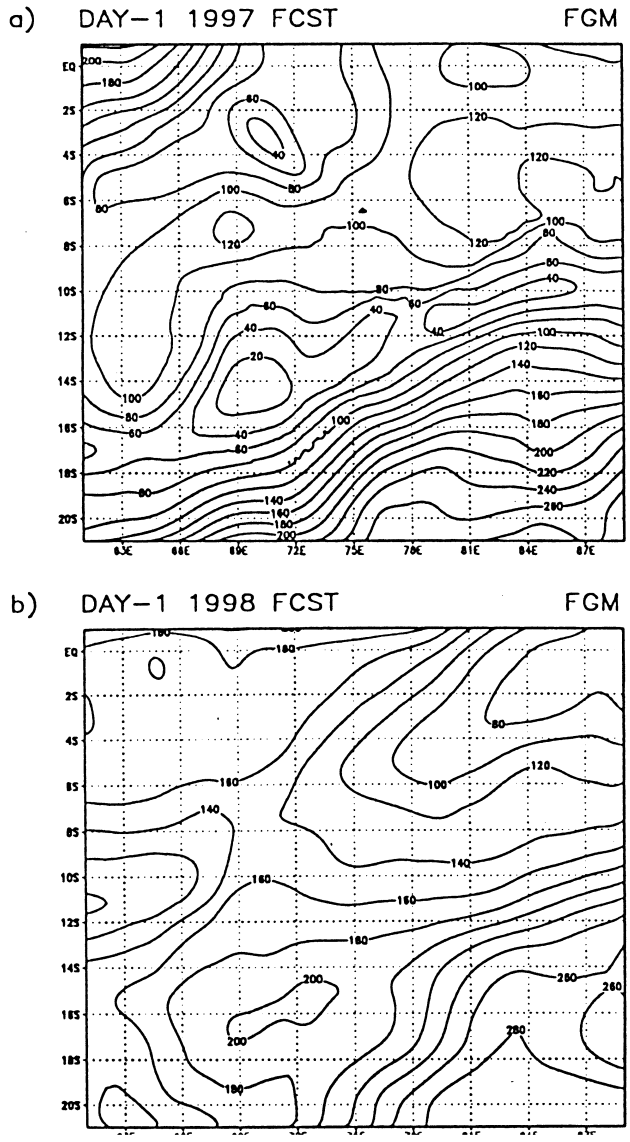

Figure 13
Distributions of simulated mean surface totoal (latent plus sensible) heat flux (Wm^{-2}) over the FGM domain with 0.17° × 0.17° resolution for 00 UTC 30 January, 1997 (a) and 00 UTC 30 January, 1998 (b).

responsible for this failure, among others are the deficiencies in diabatic heating which lead to heat sources developing at incorrect locations and times (PURI, 1994). Although the mean circulations were not correctly simulated, the rainfall could still

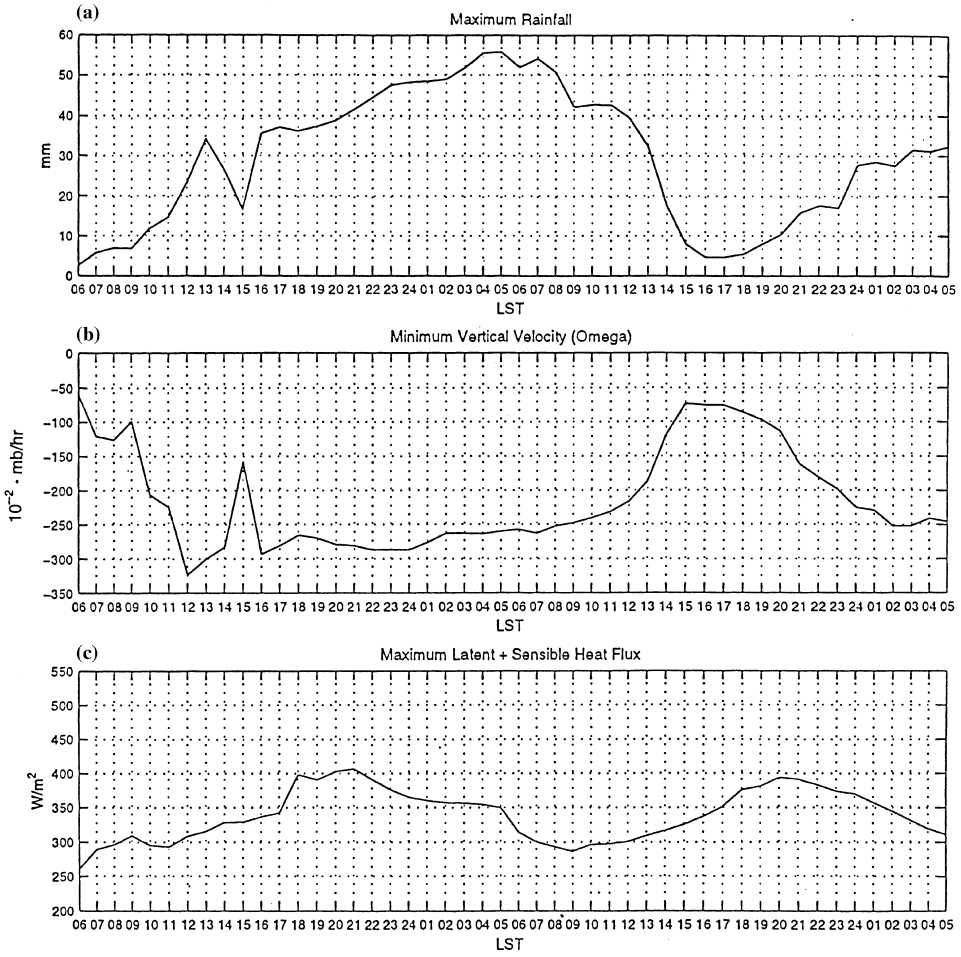

Figure 14
Diurnal variations of simulated maximum rainfall (a), minimum vertical velocity (b) and maximum total heat flux (c) as a function of Local Solar Time (LST) for 29–31 January, 1997 as derived from the FGM domain.

be predicted fairly well. Prominent diurnal cycles over the Indian Ocean were apparent in the convective zone.

During the northeast monsoon episode in the 1998 El Niño event, the model was able to simulate anomalous easterly winds and rainfall quite accurately up to a 48-hour simulation. Steady mean wind circulations during the simulation period could be attribute to a better performance of the model. Lack of surface kinetic energy and heat flux gradients over the central-eastern Indian Ocean, due to a strong subsidence branch of the Walker circulation, strongly affected low rainfall rates.

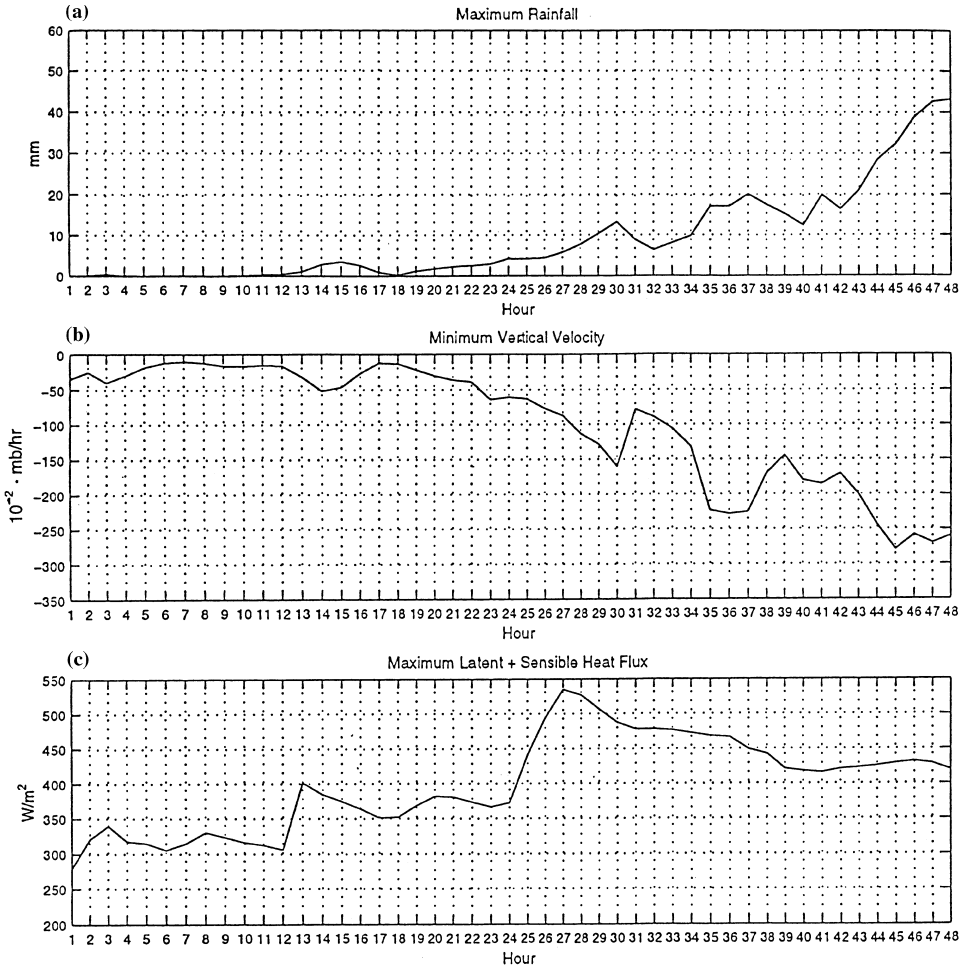

Figure 15
As in Figure 14, except for 29–31 January, 1998.

Moreover, in the region of very little convective activity, diurnal variations were not significant.

Acknowledgements

This work was partially funded by National Science Foundation under grant ATM 9632390 and the NRL cooperative project. The computations were performed at the North Carolina and NCAR Supercomputing Center. We would like to thank Dr. Yihua Wu for his contributions to algorithms used in this study.

References

ANTHES, R. A. (1977), *A Cumulus Parameterization Scheme Utilizing a One-dimensional Cloud Model*, Mon. Wea. Rev. *105*, 270–286.

BANTZER, C. H., and WALLACE, J. M. (1996), *Intraseasonal Variability in Tropical Mean Temperature and Precipitation and their Relation to the Tropical 40–50 Day Oscillation*, J. Atmos. Sci. *53*, 3032–3045.

BLACKADAR, A. K. (1976), *Modeling the Noctural Boundary Layer*, Preprints of Third Symposium on Atmospheric Turbulence, Diffusion, and Air Quality, Raleigh, NC, October 19–22 1976, Amer. Meteor. Soc. Boston, pp. 46–49.

BONY, S., LAU, K.-M., and SAD, Y. C. (1997), *Sea-surface Temperature and Large-scale Circulation Influences on Tropical Greenhouse Effect and Cloud Radiative Forcing*, J. Climate *10*, 2055–2077.

BUSINGER, J. A., WYNGAARD, J. C., IZUMI, Y., and BRADLEY, E. F. (1971), *Flux-profile Relationship in the Atmospheric Surface Layer*, J. Atmos. Sci. *28*, 181–189.

CHANG, A. T. C., CHIU, L. S., and YANG, G. (1995), *Diurnal Cycle of Oceanic Precipitation from SSM/I Data*, Mon. Wea. Rev. *123*, 3371–3380.

DAVIES, H. C. (1976), *A Lateral Boundary Formulation for Multi-level Prediction Models*, Quart. J. Roy. Meteor. Soc. *102*, 405–418.

DAVIES, H. C. (1983), *Limitations of Some Common Lateral Boundary Scheme Used in Regional NWP Models*, Mon. Wea. Rev. *11*, 1002–1012.

DUDHIA, J. (1989), *Numerical Study of Convection Observed during the Winter Monsoon Experiment Using a Mesoscale Two-dimensional Model*, J. Atoms. Sci. *46*, 3077–3107.

EMANUEL, K. A., and RAYMOND, D. J. eds. (1994), *The Representation of Cumulus Convection in Numerical Models*, MM No. 46. Am. Meteo. Soc., 246 pp.

GAUTIER, C., PETERSON, P., and JONES, C. (1998), *Variability of Air-sea Interactions over the Indian Ocean Derived from Satellite Observations*, J. Climate *11*, 1859–1873.

HOLT, T., and RAMAN, S. (1998), *A Review of Comparative Evaluation and Multilevel Boundary Layer Parameterizations for First-order and Turbulent Kinetic Energy Closure Schemes*, Rev. Geophys. *26*, 761–780.

KITOH, A. (1992), *Simulated Interannual Variations of the Indo-Australian Monsoon*, J. Meteor. Soc. Japan *70*, 563–583.

KRISHNAMURTI, T. N., KANAMITSU, M., KOSS, W. J., and LEE, J. D. (1973), *Tropical East-west Circulations during Northern Winter*, J. Atmos. Sci. *30*, 780–787.

KRISHNAMURTI, T. N., SINHA, M. C., JHA, B., and MOHANTY, U. C. (1998), *A Study of South Asia Monsoon Energetics*, J. Atmos. Sci. *55*, 2530–2548.

KUO, H. L. (1974), *Further Studies of the Parameterization of the Influence of Cumulus Convection of Large-scale Flow*, J. Atmos. Sci. *31*, 1232–1240.

LAU, K.-M. (1982), *Equatorial Response to Northeasterly Cold Surges during Winter Monsoon as Inferred from Satellite Cloud Imageries*, Mon. Wea. Rev. *110*, 1306–1313.

LAU, K.-M., and CHAN, P. H. (1985), *Aspects of the 40–50 Day Oscillation during Northern Winter as Inferred from Outgoing Longwave Radiation*, Mon. Wea. Rev. *113*, 1889–1909.

LAU, K.-M., CHANG, C.-P., *Monsoon Meteorology*, (Oxford University Press, (1987)) 161 pp.

LAU, K.-M., WU, H.-T., and BONY, S. (1997), *The Role of Large-scale Atmospheric Circulation in the Relationship between Tropical Convection and Sea-surface Temperature*, J. Climate *10*, 381–392.

LAU, K.-M., HO, C.-H., and KANG, I.-S. (1998), *Anomalous Atmospheric Hydrologic Processes Associated with ENSO: Mechanisms of Hydrologic Cycle-radiation Interaction*, J. Climate *11*, 800–815.

LI, C. (1990), *Interaction between Anomalous Winter Monsoon in East Asia and El Niño Event*. Adv. Atmos. Sci. *7*, 36–46.

MADALA, R. V., CHANG, S. W., MOHANTY, U. C., MADAN, S. C., PALIWAL, R. K., SARIN, V. B., HOLT, T., and RAMAN S. (1987), *Description of the Naval Research Laboratory Limited Area Dynamical Weather Prediction Model*, NRL Memo. Rep., No. 5992, Naval Research Laboratory, Washington, D. C., pp 131.

MADDEN, R., and JULIAN, P. (1971), *Detection of a 40–50 Day Oscillation in the Zonal Wind*, J. Atmos. Sci. *28*, 702–708.

MADDEN, R., and JULIAN, P. (1972), *Description of Global Scale Circulation cells in the Tropics with a 40–50 day period*, J. Atmos. Sci. *29*, 1109–1123.

MANABE, S., SMAGORINSKY, J., and STRICKLER, R. F. (1965), *Simulated Climatology of General Circulation Model with a Hydrological Cycle*, Mon. Wea. Rev. *93*,769–798.

MEEHL, G. A. (1987), *The Annual Cycle and Interannual Variability in the Tropical Pacific and Indian Ocean Regions*, Mon. Wea. Rev. *115*, 27–50.

MEEHL, G. A., and ARBLASTER, J. M. (1998), *The Asian-Australian Monsoon and El Niño-Southern Oscillation in the NCAR Climate System Model*, J. Climate *11*, 1356–1385.

MONIN, A. S., and YAGLOM, A. M., *Statistical Fluid Mechanics. vol. 1.* (MIT Press Cambridge, MA) 468–504.

NICHOLLS, N. (1989), *Sea-surface Temperatures and Australian Winter Rainfall*, J. Climate *2*, 965–973.

NOILHAN, J., and PLANTON, S. (1989), *A simple Parameterization of Land surface Processes for Meterological Models*, Mon. Wea. Rev. *117*, 536–549.

PURI, K. (1994), *Modeling Studies on the Australian Summer Monsoon*, Mon. Wea. Rev. *122*, 2816–2837.

SAJI, N. H., GOSWAMI, B. N., VINAYACHANDRAN, P. N., and YANMAGATA, T. (1999), *A Dipole Mode in the Tropical Indian Ocean*, Nature *401*, 360–363.

SHARMA, A. K., CHANG, A. T. C., and WILHEIT, T. W. (1991), *Estimation of Diurnal Cycle of Oceanic Precipitation from SSM/I Data*, Mon. Wea. Rev. *119*, 2168–2175.

SLINGO, J. M., MOHANTY, U. C., TIEDTKE, M., and PEARCE, R. P. (1998), *Prediction of the 1979 Summer Monsoon Onset with Modified Parameterization Schemes*, Mon. Wea. Rev. *116*, 328–346.

VINCENT, D. G. (1994), *The South Pacific Convergence Zone (SPCZ): A Review*, Mon. Wea. Rev. *122*, 1949–1970.

WEBSTER, P. J., MOORE, A. M., LOSCHNIGG, J. P., and LEBEN, R. R. (1999), *Coupled Ocean-atmosphere Dynamics in the Indian Ocean during 1997–98*, Nature *401*, 356–360.

WRIGHT, P. B., WALLACE, J. M., MITCHELL, T. P., and DESER, C. (1988), *Correlation Structure of the El Niño/Southern Oscillation Phenomenon*, J. Climate *1*, 609–625.

ZANG, G. J. (1994), *Effects of Cumulus Convection of the Simulated Monsoon Circulation in a General Circulation Model*, Mon. Wea. Rev. *122*, 2022–2038.

ZWIERS, F. W. (1993), *Simulation of the Asian Monsoon with the CCC GCM-1*, J. Climate *6*, 470–486.

(Received July 22, 1999, accepted June 20, 2000)